

A Model of Barchan Dunes Including Lateral Shear Stress

V. Schwämmle¹ and H.J. Herrmann^{1,2}

¹ Institute for Computer Applications 1, University of Stuttgart, Pfaffenwaldring 27, D-70569 Stuttgart, Germany

² Departamento de Física, Universidade Federal do Ceará, 60455-970 Fortaleza, Brazil

Abstract. Barchan dunes are found where sand availability is low and wind direction quite constant. The two dimensional shear stress of the wind field and the sand movement by saltation and avalanches over a barchan dune are simulated. The resulting final shape is compared to the results of a model with a one dimensional shear stress. A characteristic edge at the center of the windward side is discovered which is also observed for big barchans. Diffusion effects reduce this effect for small dunes.

PACS. 47.54.+r Pattern selection and formation – 45.70.-n Granular systems – 92.10.Wa Sediment transport – 92.60.Gn Winds and their effects – 91.10.Jf Topography; geometric observations – 92.40.Gc Erosion and sedimentation

1 Introduction

Barchan dunes are highly mobile dunes which constitute a considerable threat to infrastructure in arid regions with sand. They move over roads, pipelines and cover even cities. The large time scales involved considerably complicate reliable measurements. Nevertheless, over many decades measurements have been made of dunes all over the world [4, 3, 6, 16, 20, 11, 12, 7, 26, 14, 33, 10, 31, 13, 24, 22]. In order to learn more about the mechanism driving dune morphology and dynamics numerical models have been proposed [34, 35, 5, 28, 19, 29, 30, 8, 18, 23, 15, 25]. The models revealed many interesting results and raised new questions which have to be answered. The inclusion of the lateral component of the shear stress of the wind field over a barchan dune leads to the results presented in this paper.

The following section will explain some aspects concerning barchan dunes. The model will be introduced in order to simulate barchan dunes. In the following section scaling relations calculated with the model will be presented and compared to measurements. The difference between the numerical results and real dune shapes for small barchans will lead to an inclusion of diffusion in the saltation transport calculation. The last section will be about barchanoids.

2 Basics

The word *barchan* comes from the turkish language and means “active dune”. It was preserved in the scientific literature to name the isolated crescent-shaped mobile dune. Less than 1% of all dune sand on Earth is contained in barchan dunes. These dunes exist mainly in areas where not very much sand is available and wind stays unidirectional.

The size of barchans varies from heights of some meters (Figure 1) to over 50 m (Figure 2). Barchan dunes are not exactly shape invariant. There is a minimal height of 1-2 meters below which it loses its sand and no stable shape is reached. Dune shapes seem to be controlled by the saturation length of the saltation transport on the windward side [23, 9]. This is the distance needed to reach the saturated sand flux over a sandy surface. The saturation length, not to be confused with the saltation length (mean length of a grain trajectory in air), has a complex dependency on the air shear stress. Zero flux over a ground without sand bed needs a transient length to reach a saturated flux at the place where the surface begins to be covered with sand.

Small stable barchan dunes have a short slip face and the crest does not coincide with the brink. Whereas the sand is trapped completely in the slip face, the lack of a slip face at the horns allows the sand grains to leave the dune there. Thus a barchan dune grows if sand influx is larger than outflux and vice versa.

3 The model

The model described here can be seen as a minimal model including the main processes of dune morphology. As predecessors of the model described here the works of [21] and [25] revealed interesting new insights into dynamics and formation of dunes. The model of [25], modelling transverse dunes, will be used here to obtain the steady state of barchan dunes. The simulations are carried out with a completely unidirectional and constant wind source. In this article the model is used to simulate isolated single barchan dunes. In every iteration the horizontal shear stress τ of the wind, the saltation flux \mathbf{q} and the flux due

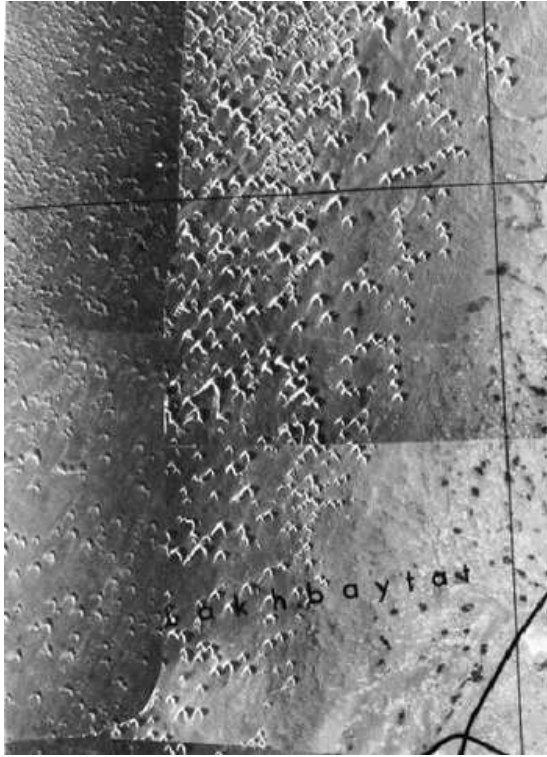


Fig. 1. Aerial photograph of the dune field north of Laâyoune, Morocco. The dune heights are of some meters. The wind is blowing from NNE to SSW (photo taken from Sauer-
mann (2001)).



Fig. 2. Aerial photograph of the dune field of Jericoacoara near Fortaleza, Brazil. Some dunes are over 50 meters high. Photo taken from Jimenez et al (1999).

to avalanches are calculated. The time scale of these processes is much shorter than the time scale of changes in the dune surface so that they are treated to be instantaneous. In the following the different steps at every iteration are explained.

The air shear stress τ at the ground: We use the well known logarithmic velocity profile of the atmospheric bound-

ary layer as a basis of our shear stress calculation,

$$v(z) = \frac{u_*}{\kappa} \ln \frac{z}{z_0}, \quad (1)$$

where $v(z)$ is the horizontal wind velocity, z_0 the roughness length, giving a measure of the roughness of the surface, and $u_* = \sqrt{\tau/\rho}$ is called shear velocity. Although it has the dimension of a velocity the shear velocity u_* is used as a measure for the shear stress. The shear stress perturbation over a single dune or over a dune field given by the height $h(x, y)$ is calculated using the algorithm of [32]. The τ_x -component points in wind direction and the τ_y -component denotes the lateral direction perpendicular to the wind. The calculation is made in Fourier space, k_x and k_y are the wave numbers,

$$\hat{\tau}_x(k_x, k_y) = \frac{h(k_x, k_y)k_x^2}{|k|} \frac{2}{U^2(l)} \left(1 + \frac{2 \ln L |k_x| + 4\gamma + 1 + i \operatorname{sign}(k_x)\pi}{\ln l/z_0} \right), \quad (2)$$

and

$$\hat{\tau}_y(k_x, k_y) = \frac{h(k_x, k_y)k_x k_y}{|k|} \frac{2}{U^2(l)}, \quad (3)$$

where $|k| = \sqrt{k_x^2 + k_y^2}$ and $\gamma = 0.577216$ (Euler's constant). $U(l)$ is the normalized velocity of the undisturbed logarithmic profile at the height of the inner region l [21] defined in [32]. The values of the roughness length z_0 and the so called characteristic length L were adjusted to the data of [24] supposing we have an averaged shear velocity of $u_* = 0.5 \text{ ms}^{-1}$ in the region where the measurements were carried out. Thus z_0 is set to 0.0025 m and L to 10 m.

Equations (2) and (3) are calculated in Fourier space and have to be multiplied with the logarithmic velocity profile of Equation (1) in real space in order to obtain the total shear stress. The surface is assumed to be instantaneously rigid and the effect of sediment transport is incorporated in the roughness length z_0 . For slices in wind direction the separation streamlines in the lee zone of the dunes are fitted by a polynomial of third order attaching to the brink continuously. The length of the separation streamlines is determined by allowing a maximum slope of 14° [21]. The separation bubble guarantees a smooth surface for the wind field calculation and the shear stress in the area inside the separation bubble is set equal to zero. Problems can arise due to numerical fluctuations in the value of the windward slope at the brink where the separation bubble begins and its influence on the calculation of the separation streamline for each slice. To get rid of this numerical error the surface is Fourier-filtered by cutting the small frequencies.

The saltation flux q : The product of the sand density and the sand velocity leads to the sand flux over the surface,

$\mathbf{q}(x, y) = \mathbf{u}(x, y)\rho(x, y)$. The saltation flux is calculated from mass conservation,

$$\frac{\partial \rho(x, y, t)}{\partial t} + \nabla \rho(x, y, t) \mathbf{u}(x, y, t) + C_{diff} \Delta \rho(x, y, t) = \Gamma(x, y, t), \quad (4)$$

where ρ is the density and \mathbf{u} the velocity of the sand grains in the saltation layer. These variables are integrated over the vertical component. C_{diff} denotes a diffusion constant which will be the crucial parameter in Section 5. In the other chapters C_{diff} is set to zero. Grains are entrained by the air and deposited on the sand bed which is expressed by the exchange term Γ . The velocity of the sand grains is calculated from momentum conservation,

$$\frac{\partial \mathbf{u}(x, y, t)}{\partial t} + (\mathbf{u}(x, y, t) \nabla) \mathbf{u}(x, y, t) = \frac{1}{\rho(x, y, t)} (\mathbf{f}_{drag}(x, y, t) + \mathbf{f}_{bed}(x, y, t) + \mathbf{f}_g(x, y)). \quad (5)$$

The drag force \mathbf{f}_{drag} denotes the interaction between air flow and sand grains, \mathbf{f}_{bed} is the deceleration of the grains by the collision with the sand bed and \mathbf{f}_g is the gravity force which drives the grains into the direction of the steepest gradient of the height profile. The time to reach the steady state of sand flux over a new surface is several orders of magnitude shorter than the time scale of the surface evolution. Hence, the steady state is assumed to be reached instantaneously. The characteristic length scale to reach a saturated saltation layer influences the calculation by breaking the scale invariance of dunes and by determining the minimal size of a barchan dune [23].

A calculation of the saltation transport by the well known flux relations [1, 17, 27] would restrict the model to saturated sand flux which is not the case observed at the foot of the windward side of a barchan dune due to the reduced sand supply. We simplified the closed model of [23], resulting from Equation (4) and (5), by neglecting the time dependent terms and the convective term of the grain velocity $\mathbf{u}(x, y)$. This yields Equations (6) and (8) where ρ and \mathbf{u} are determined from the shear stress obtained before and the gradient of the actual surface,

$$\text{div}(\rho \mathbf{u}) + C_{diff} \Delta \rho = \frac{1}{T_s} \rho \left(1 - \frac{\rho}{\rho_s} \right) \begin{cases} \Theta(h) & \rho < \rho_s \\ 1 & \rho \geq \rho_s \end{cases}, \quad (6)$$

with

$$\rho_s = \frac{2\alpha}{g} (|\boldsymbol{\tau}| - \tau_t) \quad T_s = \frac{2\alpha|\mathbf{u}|}{g} \frac{\tau_t}{\gamma(|\boldsymbol{\tau}| - \tau_t)}. \quad (7)$$

and

$$\frac{3}{4} C_d \frac{\rho_{air}}{\rho_{quartz}} d^{-1} (\mathbf{v}_{eff} - \mathbf{u}) |\mathbf{v}_{eff} - \mathbf{u}| - \frac{g}{2\alpha} \frac{\mathbf{u}}{|\mathbf{u}|} - g \nabla h = 0, \quad (8)$$

where v_{eff} is the velocity of the grains in the saturated state,

$$\mathbf{v}_{eff} = \frac{2\mathbf{u}_*}{\kappa|\mathbf{u}_*|}.$$

$$\left(\sqrt{\frac{z_1}{z_m} u_*^2 + \left(1 - \frac{z_1}{z_m} \right) u_{*t}^2} + \left(\ln \frac{z_1}{z_0} - 2 \right) \frac{u_{*t}}{\kappa} \right), \quad (9)$$

and

$$u_* = \sqrt{\tau/\rho_{air}} \quad (10)$$

In Equation (8) the force terms are arranged in the same order as in Equation (5). The constants and model parameters have been taken from [23] and are summarized here: $g = 9.81 \text{ m s}^{-2}$, $\kappa = 0.4$, $\rho_{air} = 1.225 \text{ kg m}^{-3}$, $\rho_{quartz} = 2650 \text{ kg m}^{-3}$, $z_m = 0.04 \text{ m}$, $z_0 = 2.5 \cdot 10^{-5} \text{ m}$, $D = d = 250 \mu\text{m}$, $C_d = 3$, $u_{*t} = 0.28 \text{ m s}^{-1}$, $\gamma = 0.4$, $\alpha = 0.35$ and $z_1 = 0.005 \text{ m}$.

Avalanches: Surfaces with slopes which exceed the maximal stable angle of a sand surface, the called *angle of repose* $\Theta \approx 34^\circ$, produce avalanches which slide down in the direction of the steepest descent. The unstable surface relaxes to a somewhat smaller angle. For the study of dune formation two global properties are of interest. These are the sand transport downhill due to gravity and the maintenance of the angle of repose. To determine the new surface after the relaxation by avalanches the model proposed by [2] is used. For the equations see [25]. Like in the calculation of the sand flux the steady state of the avalanche model is assumed to be reached instantaneously. Hence, we can neglect the time dependent terms. In the dune model a certain amount of sand is transported over the brink to the slip face and in every iteration the sand excess is relaxed over the slip face by this avalanche model determining the steady state.

The time evolution of the surface The calculation of the sand flux over a not stationary dune surface leads to changes by erosion and deposition of sand grains. The change of the surface profile can be calculated using the conservation of mass,

$$\frac{\partial h}{\partial t} = -\frac{1}{\rho_{sand}} \nabla \mathbf{q}. \quad (11)$$

Finally, it is noted that Equation (11) is the only remaining time dependent equation and thus defines the characteristic time scale of the model which is normally between 3–5 hours for every iteration.

The initial surface and boundary conditions: The genesis of a dune is still not known very well. Hence, the simulations must start with an essentially arbitrary initial surface. We can then observe how the system reaches

a final steady state. A steady state means that the dune shape does not undergo temporal changes anymore.

As initial surface we take a flat bed of solid ground with a Gaussian hill of sand on it. The maximum slope of the Gaussian is restricted in order to stay within the approximations of the shear stress calculation.

We use quasi-periodic boundary conditions, i.e. the sand outflux at the outlet of the simulation field is integrated and the same amount of sand enters the field inlet as a constant influx. Neglecting the amount of sand leaving the simulation area by the lateral boundary, the sand volume is conserved.

4 Scaling laws

In this section the morphologic relationships between height h , width w , length l and velocity v_d of barchan dunes resulting of the simulations are presented. The shapes for different dune sizes are compared. Therefore calculations of dunes which have different sizes were performed for the shear velocities $u_* = 0.4 \text{ ms}^{-1}$, $u_* = 0.45 \text{ ms}^{-1}$ and $u_* = 0.5 \text{ ms}^{-1}$. Single isolated barchan dunes are modeled using a quasi-periodic boundary until the final steady shape is reached.

Height, width and length relationships: Linear relationships between height, width and length were observed by [4] and [10] for barchans in southern Peru and by [8] in Morocco. Figures 3 and 4 depict the height width and the height length relationships for different shear velocities, respectively.

A linear relationship is obtained for dunes larger than 2–3 meters. The linearity is valid only for length scales much larger than the saturation length ($l \gg l_s$). The functional dependence of the saturation length on the shear velocity predicts larger width and length for a dune of the same height, for decreasing shear velocities. This is in agreement with [23] who found an increase of l_s at the shear velocity threshold.

The asymptotic slopes of the linear relationships are not affected by different shear velocities. The results are compared to the data of [8] (Figures 3 and 4). The data of the barchans of Morocco fit best to the simulation results for a shear velocity $u_* = 0.5 \text{ ms}^{-1}$. Table 1 compares the slope a_W and the axis intercept b_W of the linear relationships to the data of [8], [6] and [4].

Dune velocity: According to [21] the dune velocity decreases inversely proportional to the length of the envelope of the surface formed by the height profile and the separation bubble. The separation bubble of the barchans in the dune model described here fills almost exactly the region between the horns so that the length l of the dune can be used in order to evaluate the simulation results. Thus Bagnold’s law, the reciprocal proportionality of the dune velocity v_d to the height h , has to be modified, to

$$v_d = \frac{\Phi_{dune}}{l} \quad (12)$$

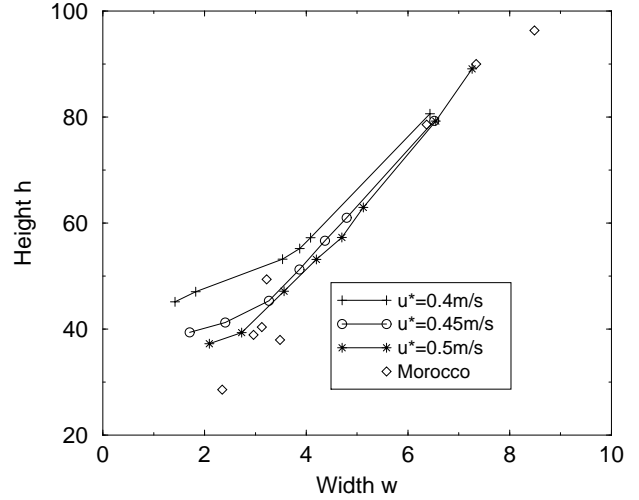


Fig. 3. Height width relation of dunes in Morocco (diamonds) and the results of numerical calculations for different shear velocities.

where Φ_{dune} is in principle dependent on the shear velocity. The relation between dune velocity and height revealed the same deviations from Bagnold’s law for small dunes as in the case of the height length relationship (Figure 4). Figure 5 depicts the dune velocity v_d versus dune length l . The surprising result is that the dune velocity does not differ from Equation 12 even for small dune sizes and so the saturation length seems to have no influence on the dune velocity.

The shape: Barchans are not really shape invariant due to the important role of the saturation length of the saltation transport. Nevertheless the shapes of barchans of different sizes are compared in order to obtain more information about the deviation from shape invariance. [8] fitted the normalized transversal profile of the measured dunes in Morocco with a parabola. [21] found a good agreement of the normalized transversal profile of his numerical calculations (neglecting the lateral shear stress) to a parabola. Following his work the axes are rescaled and dimensionless variables are introduced,

$$\tilde{x} = \frac{1}{l}x \quad \tilde{y} = \frac{1}{w}y \quad \tilde{z} = \frac{1}{h}z. \quad (13)$$

Table 1. Height and width relationship.

	a_W	b_W
Finkel	10.3	4.0
Hastenrath	8.2	9.5
Herrmann	11.1	5.6
Simulations:		
$u_* = 0.4 \text{ ms}^{-1}$	9.9	16.6
$u_* = 0.45 \text{ ms}^{-1}$	10.6	10.4
$u_* = 0.5 \text{ ms}^{-1}$	10.5	8.5

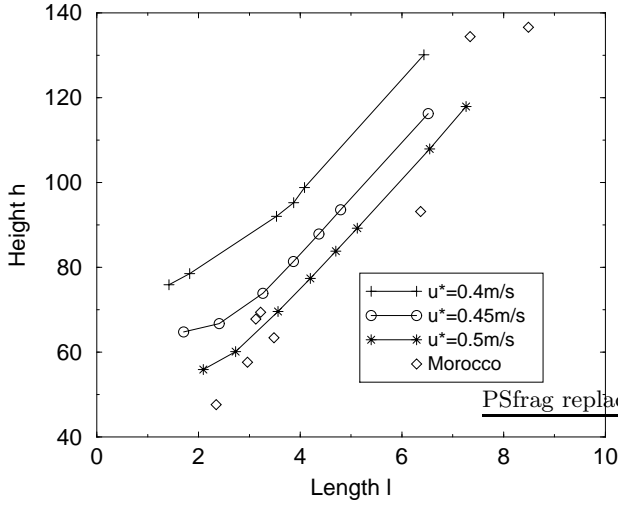


Fig. 4. Height length relation of dunes in Morocco (diamonds) and the results of numerical calculations for different shear velocities.

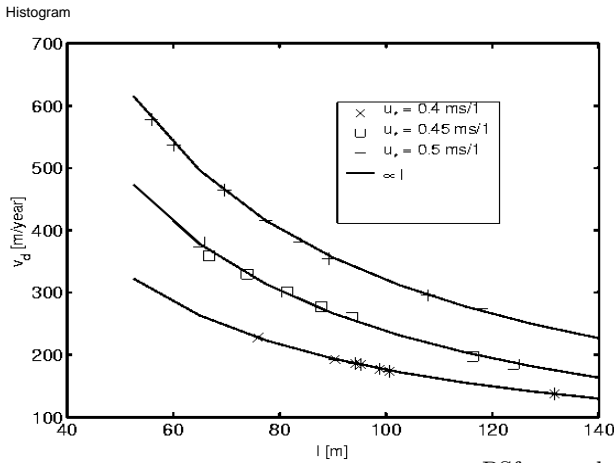


Fig. 5. The velocity v_d of barchans fits very well to their reciprocal length. Note: The velocity is assumed to be constant for 365 days of wind per year and is thus smaller in real conditions.

Figure 6 shows our normalized transversal profiles compared with the field data of [21]. In Figure 7 we compare the results of the normalized transversal profiles with a fit to a parabola. The upper part of the profile fits quite well whereas the lower part is far away from a parabola. We searched for a better fit with another function. Figures 7 and 8 indicate that the powers of a cosh-function fit quite well, even the longitudinal profile. The inclusion of lateral shear stress in the model seems to lead qualitatively at least for the transversal cuts to a change from a parabolic to a \cosh^2 -profile. In Figure 8 the slope at the brink at the windward side decreases for larger dunes. Finally the shapes of a 45 and a 5 meter high dune are depicted in Figure 9. The slip face of larger dunes cuts a larger piece from the dune body.

In figure 9 we can see a rather sharp edge in the shape at the center of the windward side which is not observed in the results of the dune model of [21]. The inclusion of

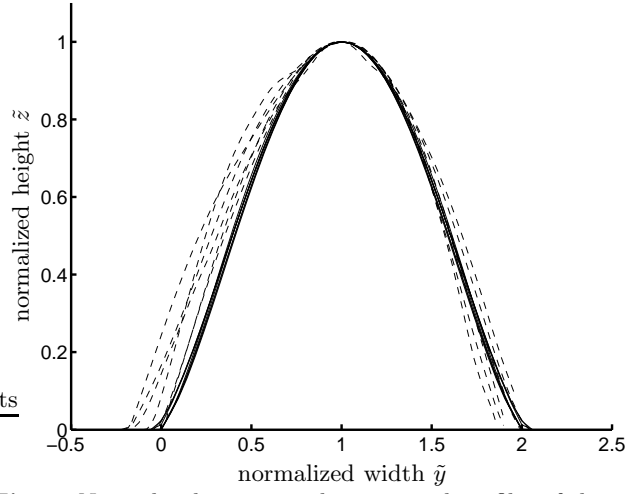


Fig. 6. Normalized superposed transversal profiles of the simulations (solid lines) and normalized transversal profiles of the dunes measured in Morocco from Herrmann and Sauermann (2000) (dashed lines). The shear velocity in the simulations is $u_* = 0.5 \text{ms}^{-1}$.

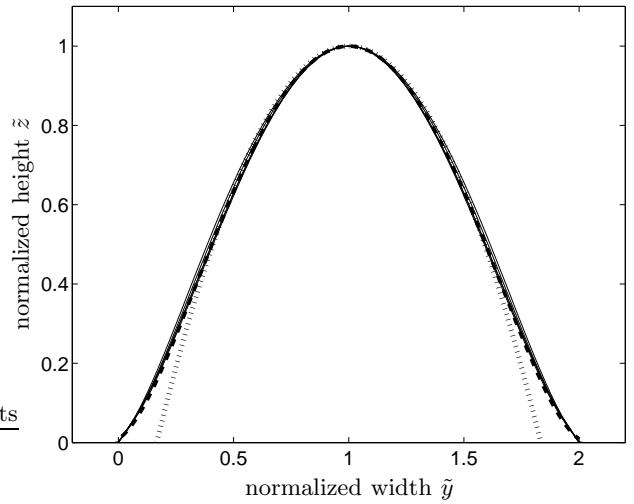


Fig. 7. Normalized transversal profiles of the dunes. A fit with $\cosh^2(x)$ is given by the dashed line and fits much better than a parabola (dotted line). The shear velocity is $u_* = 0.5 \text{ms}^{-1}$.

the lateral component in the shear stress calculation seems responsible for this difference. This edge has not been observed for small dunes, for example in Morocco. But the large dunes in Figure 2 show a very similar edge. Exact measurements of the shape of a large barchan would reveal more information and hopefully validate the model results. We assume that the absence of the edge for small dunes can be explained by diffusion-like smoothing effects occurring during the saltation transport. Diffusion which in the simulations depicted so far has not been considered acts on small scales and for larger scales the influence of diffusion on the dune shape should be negligible. In the next section the shapes obtained from the model are studied for different diffusion constants.

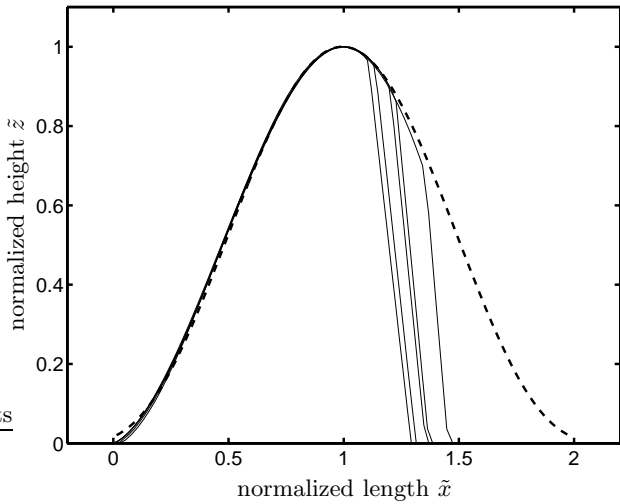


Fig. 8. Normalized longitudinal profiles of the dunes. A fit with $\cosh^4(x)$ (dashed line) reproduces quite well the windward side. The shear velocity is $u_* = 0.5\text{ms}^{-1}$.

5 The effect of diffusion

The dune model including the lateral component of the shear stress revealed a characteristic shape with a rather sharp edge on the windward side which is not found for small barchan dunes for example in Morocco. To better understand this effect we simulate barchan dunes of about 12 meters height having the same volume with different diffusion constants C_{diff} . For larger dunes and therefore larger length scales the effect of diffusion transport will be weaker and the final state calculated by the dune model without diffusion should match real dune shapes.

The results in this section can be discussed only qualitatively due to the fact that experimentally the diffusion constant is unknown. Figures 10 and 11 show the contour lines of the height profile and the sand density in the saltation layer, respectively. Very high diffusion constants like the one of the bottom part of these figures show that the sharp edge in the shape of the windward side is smoothed. The sand density in the saltation layer is flattened out as can be expected from diffusion processes. Behind the brink always the sand density drops to zero due to the vanishing shear stress. Diffusion changes the contour lines of the shape dramatically. An estimation of the diffusion constant and precise measurements of the height profiles of small and large barchans could give more insight into the influence of diffusion on the morphology of barchan dunes in the future.

Figures 12 and 13 depict a longitudinal and a transversal profile of a barchan dune in steady state for different diffusion constants. The height and the slope at the brink decrease for a stronger diffusion. The length of the longitudinal profile increases for a larger diffusion constant whereas the width stays constant. The knowledge of C_{diff} would also help to determine more realistic values for z_0 and L (Equation (2)) by fitting them to simulation results from a model with diffusion. Consistency can be checked by comparing with higher barchans where diffu-

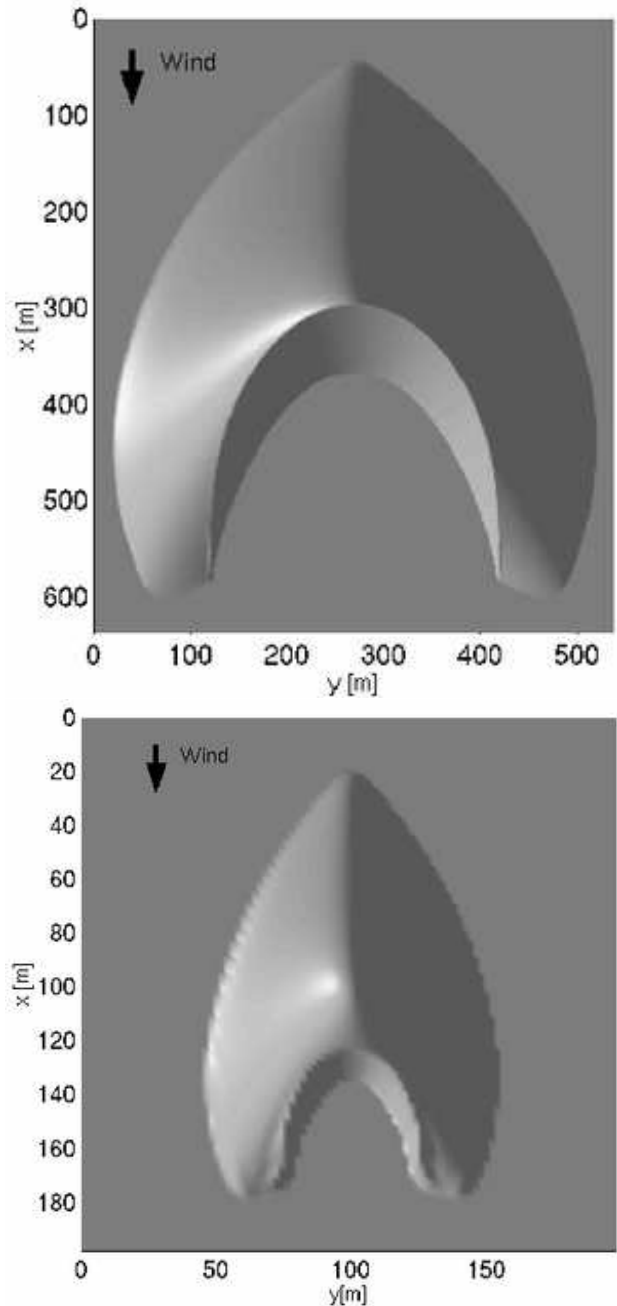


Fig. 9. On top the surface of a 45 m high barchan dune is depicted. The dune in the bottom part has a height of 5 m. There is no simple shape invariance. The shear velocity is $u_* = 0.5\text{ms}^{-1}$ for both simulations.

sion is weaker. But the computational costs and the missing measurements for large barchans (there do not exist many large barchans) make the realization still difficult at this point.

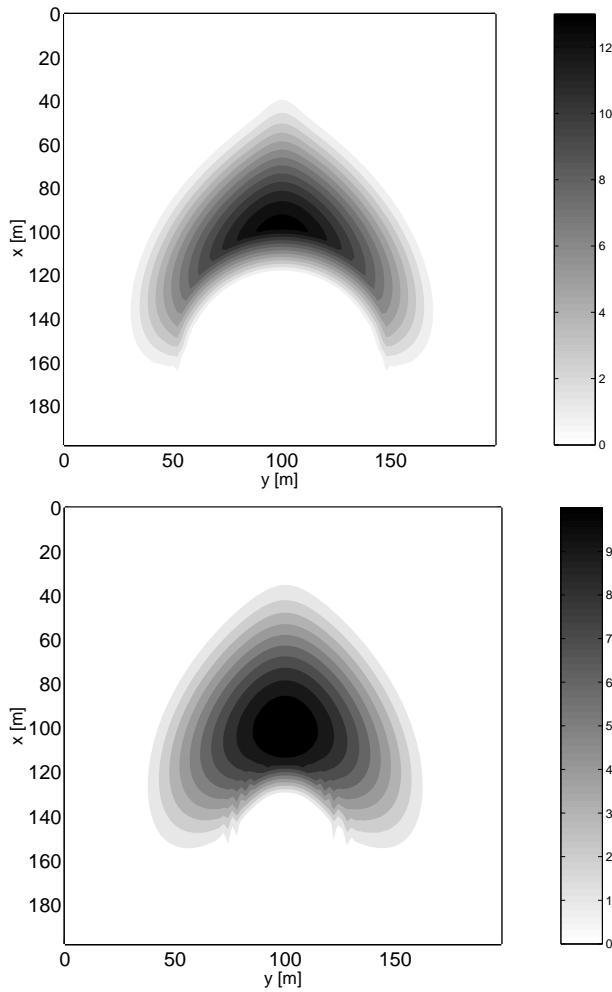


Fig. 10. Comparing the topography of two barchan dunes of equal volume in steady state calculated from the same initial surface for a diffusion constant of $C_{diff} = 0.0$ (top) and $C_{diff} = 4.0 \text{ m}^2\text{s}^{-1}$ (bottom). The shear velocity is $u_* = 0.5\text{ms}^{-1}$.

6 Barchanoids, between barchan and transverse dunes

If an area does not contain sufficient sand to form transverse dunes but too much sand is available to keep the barchans isolated from each other the barchan dunes connect and interesting hybrid forms appear, the so called barchanoids. The barchan dunes can be connected longitudinally and laterally.

Here only qualitative results will be presented. The simulation with the dune model is performed with a nearly flat initial surface (some small Gaussian hills randomly placed on a plane) of an averaged sand height of three meters. The boundary conditions are quasi periodic in wind direction and open in the lateral direction. The volume of sand in the simulation is held constant. Figures 14 and 15 show two states of the simulation. In the first figure the barchans are connected longitudinally and laterally. The barchans are growing so that the sand finally accumulates in a single row of larger dunes which are connected later-

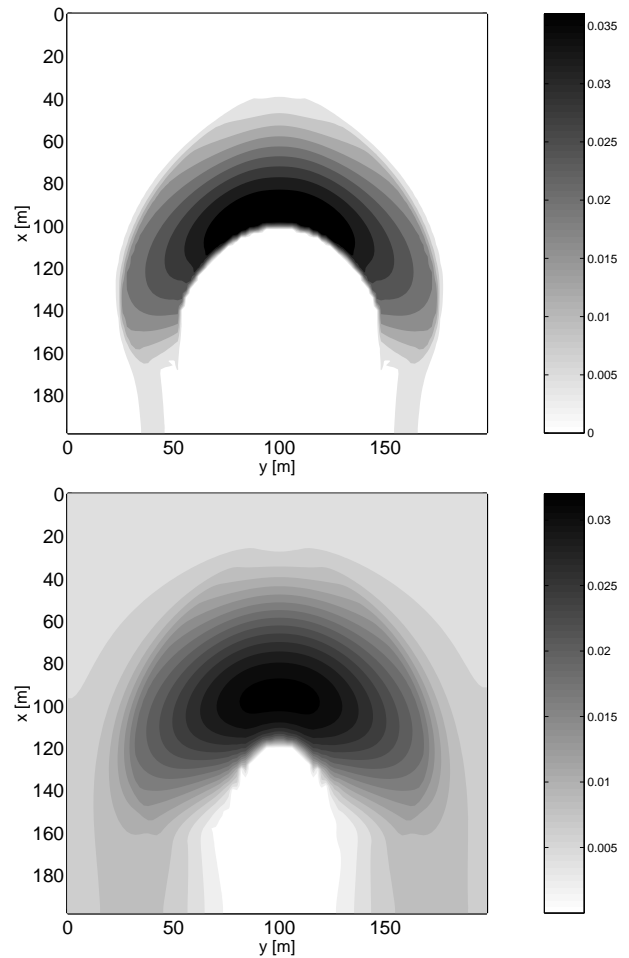


Fig. 11. Comparing the sand density ρ of the saltation layer of two barchan dunes of equal volume in steady state calculated from the same initial surface for a diffusion constant of $C_{diff} = 0.0$ (top) and $C_{diff} = 4.0 \text{ m}^2\text{s}^{-1}$ (bottom). The diffusion term smoothes the sand density in the saltation layer. The shear velocity is $u_* = 0.5\text{ms}^{-1}$.

ally. Similar barchanoids can be found for example in the dune field of Lençóis Maranhenses in Brazil where on top in the rain season the dunes can be separated by lagoons filled with rainwater (Figure 16). In this dune field the barchan dunes are connected in both directions.

7 Conclusions

The scaling laws revealed approximately linear relationships between height, width and length of the dunes. This is not valid for small dunes due to the influence of the saturation length. Bagnold's law was modified relating the dune velocity to the length of the dunes. This fit was surprisingly good and there seems to be a negligible influence of the saturation length on dune velocities. The transversal and the longitudinal cuts showed that a parabola fits less well to numerical and real data than a \sin^2 -function. The shape invariance was verified and a characteristic sharp edge of the shape at the windward side was observed in

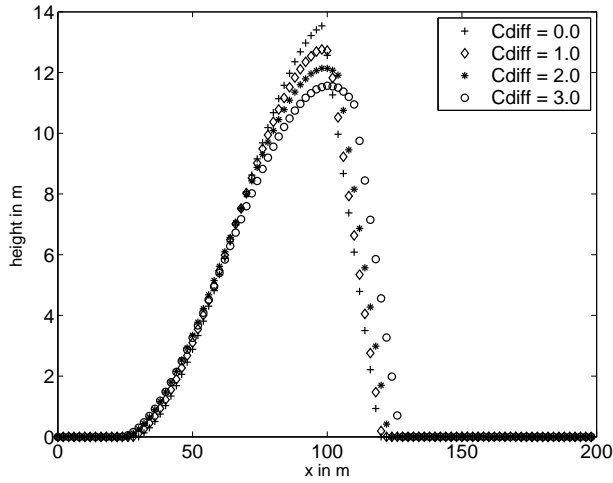


Fig. 12. The longitudinal cut through the dune for different diffusion constants C_{diff} . The length of the slip face and the slope at the brink decrease with increasing diffusion constant. The shear velocity is $u_* = 0.5\text{ms}^{-1}$.

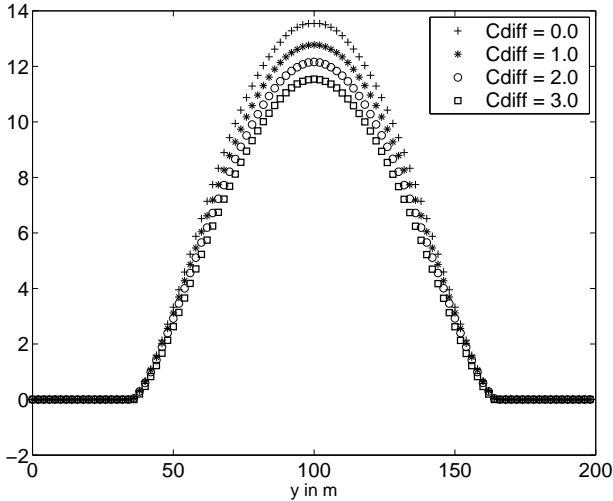


Fig. 13. The transversal cut through the windward side of the dune for different diffusion constants C_{diff} . The height of the dune decreases with increasing diffusion constant. The shear velocity is $u_* = 0.5\text{ms}^{-1}$.

the calculations. The model was applied to the same dune for different diffusion constants. The diffusion constant strongly influences the form of the final shape. Finally it was shown that barchanoids can be obtained from longitudinally and laterally connected barchans.

8 Acknowledgement

H.J. Herrmann was partially funded by the Max-Planck-price.

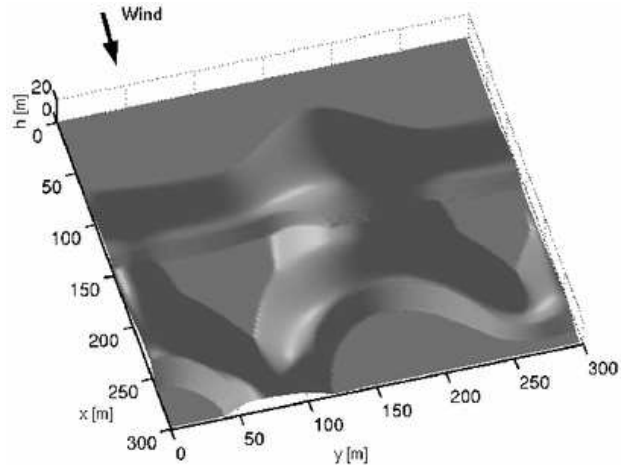


Fig. 14. A simulation with quasi-periodic boundary conditions. There is too much sand to build isolated barchans. The barchans are connected in the longitudinal and lateral direction. The shear velocity is $u_* = 0.5\text{ms}^{-1}$

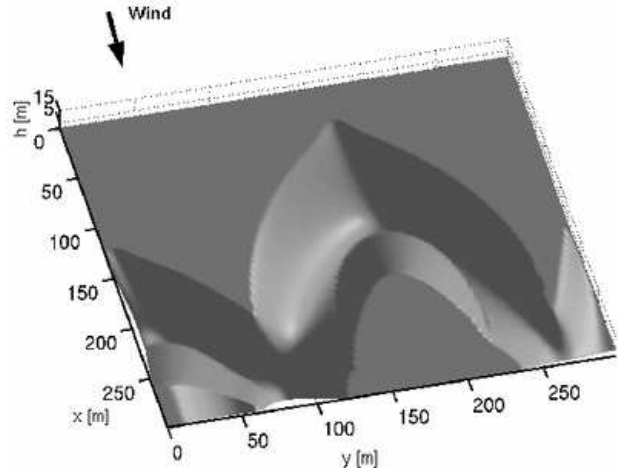


Fig. 15. Later state of the same simulation with quasi-periodic boundary conditions. Now the barchans are connected only in the lateral direction. The shear velocity is $u_* = 0.5\text{ms}^{-1}$

References

1. R. A. Bagnold. *The physics of blown sand and desert dunes*. Methuen, London, 1941.
2. J. P. Bouchaud, M. E. Cates, J. Ravi Prakash, and S. F. Edwards. Hysteresis and metastability in a continuum sandpile model. *J. Phys. France I*, 4:1383, 1994.
3. A. Coursin. Observations et expériences faites en avril et mai 1956 sur les barkhans du Souhel el Abiodh (région est de Port-Étienne). *Bulletin de l' I. F. A. N.*, 22A, no. 3:989–1022, 1964.
4. H. J. Finkel. The barchans of southern Peru. *Journal of Geology*, 67:614–647, 1959.
5. P. F. Fisher and P. Galdies. A computer model for barchan-dune movement. *Computer and Geosciences*, 14-2:229–253, 1988.
6. S. Hastenrath. The barchans of the Arequipa region, southern Peru. *Zeitschrift für Geomorphologie*, 11:300–331, 1967.



Fig. 16. Photo of the dune field of Lençóis Maranhenses, Brazil. In the rain season the inter-dune space is sometimes filled with lagoons. Barchan dunes are connected in longitudinal and lateral direction.

7. S. Hastenrath. The barchan dunes of southern Peru revisited. *Zeitschrift für Geomorphologie*, 31-2:167–178, 1987.
8. H. J. Herrmann and G. Sauer mann. The shape of dunes. *Physica A*, 283:24–30, 2000.
9. P. Hersen, S. Douady, and B. Andreotti. Relevant length-scale of barchan dunes. *Phys. Rev. L.*, 89:264301, 2002.
10. P. A. Hesp and K. Hastings. Width, height and slope relationships and aerodynamic maintenance of barchans. *Geomorphology*, 22:193–204, 1998.
11. A. D. Howard and J. B. Morton. Sand transport model of barchan dune equilibrium. *Sedimentology*, 25:307–338, 1978.
12. D. Jäkel. Die Bildung von Barchanen in Faya-Largeau/Rep. du Tchad. *Zeitschrift für Geomorphologie N.F.*, 24:141–159, 1980.
13. Jose A. Jimenez, Luis P. Maia, Jordi Serra, and Jader Morais. Aeolian dune migration along the Ceará coast, north-eastern Brazil. *Sedimentology*, 46:689–701, 1999.
14. G. Kocurek, M. Townsley, E. Yeh, K. Havholm, and M. L. Sweet. Dune and dune-field development on Padre Island, Texas, with implications for interdune deposition and water-table-controlled accumulation. *Journal of Sedimentary Petrology*, 62-4:622–635, 1992.
15. K. Kroy, G. Sauer mann, and H. J. Herrmann. Minimal model for sand dunes. *Phys. Rev. L.*, 68:54301, 2002.
16. K. Lettau and H. Lettau. Bulk transport of sand by the barchans of the Pampa de La Joya in southern Peru. *Zeitschrift für Geomorphologie N.F.*, 13-2:182–195, 1969.
17. K. Lettau and H. Lettau. Experimental and micrometeorological field studies of dune migration. In H. H. Lettau and K. Lettau, editors, *Exploring the world's driest climate*, pages 110–147. Madison, Center for Climatic Research, Univ. Wisconsin, 1978.
18. H. Momiji and A. Warren. Relations of sand trapping efficiency and migration speed of transverse dunes to wind velocity. *Earth Surface Processes and Landforms*, 25:1069–1084, 2000.
19. H. Nishimori, M. Yamasaki, and K. H. Andersen. A simple model for the various pattern dynamics of dunes. *Int. J. of Modern Physics B*, 12:257–272, 1999.
20. M. Sarnthein and E. Walger. Der äolische Sandstrom aus der W-Sahara zur Atlantikküste. *Geologische Rundschau*, 63:1065–1087, 1974.
21. G. Sauer mann. *Modeling of Wind Blown Sand and Desert Dunes*. PhD thesis, University of Stuttgart, 2001.
22. G. Sauer mann, J. S. Andrade, L.P. Maia, U.M.S. Costa, A.D. Araújo, and H. J. Herrmann. Wind velocity and sand transport on a barchan dune. *Geomorphology*, 2003.
23. G. Sauer mann, K. Kroy, and H. J. Herrmann. A continuum saltation model for sand dunes. *Phys. Rev. E*, 64:31305, 2001.
24. G. Sauer mann, P. Rognon, A. Poliakov, and H. J. Herrmann. The shape of the barchan dunes of southern Morocco. *Geomorphology*, 36:47–62, 2000.
25. V. Schwämmle and H.J. Herrmann. Modelling transverse dunes. cond-mat/0301589, 2003.
26. M. C. Slattery. Barchan migration on the Kuiseb river delta, Namibia. *South African Geographical Journal*, 72:5–10, 1990.
27. M. Sørensen. An analytic model of wind-blown sand transport. *Acta Mechanica (Suppl.)*, 1:67–81, 1991.
28. J. M. T. Stam. On the modelling of two-dimensional aeolian dunes. *Sedimentology*, 44:127–141, 1997.
29. J. H. van Boxel, S. M. Arens, and P. M. van Dijk. Aeolian processes across transverse dunes i: Modelling the air flow. *Earth Surf. Process. Landforms*, 24:255–270, 1999.
30. P. M. van Dijk, S. M. Arens, and J. H. van Boxel. Aeolian processes across transverse dunes ii: Modelling the sediment transport and profile development. *Earth Surf. Process. Landforms*, 24:319–333, 1999.
31. I. J. Walker. Secondary airflow and sediment transport in the lee of a reversing dune. *Earth Surface Processes and Landforms*, 24:437–448, 1998.
32. W. S. Weng, J. C. R. Hunt, D. J. Carruthers, A. Warren, G. F. S. Wiggs, I. Livingstone, and I. Castro. Air flow and sand transport over sand-dunes. *Acta Mechanica (Suppl.)*, 2:1–22, 1991.
33. G. F. S. Wiggs, I. Livingstone, and A. Warren. The role of streamline curvature in sand dune dynamics: evidence from field and wind tunnel measurements. *Geomorphology*, 17:29–46, 1996.
34. F. K. Wippermann and G. Gross. The wind-induced shaping and migration of an isolated dune: A numerical experiment. *Boundary Layer Meteorology*, 36:319–334, 1986.
35. O. Zeman and N. O. Jensen. Progress report on modeling permanent form sand dunes. *Risø National Laboratory*, M-2738, 1988.